Rapid Communications

Magnetoelectric effect and orbital magnetization in skyrmion crystals: Detection and characterization of skyrmions

Börge Göbel,[1,*] Alexander Mook,[1] Jürgen Henk,[2] and Ingrid Mertig[1,2]
[1]*Max-Planck-Institut für Mikrostrukturphysik, D-06120 Halle (Saale), Germany*
[2]*Institut für Physik, Martin-Luther-Universität Halle-Wittenberg, D-06099 Halle (Saale), Germany*

(Received 26 October 2017; revised manuscript received 16 May 2018; published 13 February 2019)

Skyrmions are small magnetic quasiparticles, which are uniquely characterized by their topological charge and their helicity. In this Rapid Communication, we show via calculations how both properties can be determined without relying on real-space imaging. The orbital magnetization and topological Hall conductivity measure the arising magnetization due to the circulation of electrons in the bulk and the occurrence of topologically protected edge channels due to the emergent field of a skyrmion crystal. Both observables quantify the topological Hall effect and distinguish skyrmions from antiskyrmions by sign. Additionally, we predict a magnetoelectric effect in skyrmion crystals, which is the generation of a magnetization (polarization) by application of an electric (magnetic) field. This effect is quantified by spin toroidization and magnetoelectric polarizability. The dependence of the transverse magnetoelectric effect on the skyrmion helicity fits that of the classical toroidal moment of the spin texture and allows one to differentiate skyrmion helicities: It is largest for Bloch skyrmions and zero for Néel skyrmions. We predict distinct features of the four observables that can be used to detect and characterize skyrmions in experiments.

DOI: 10.1103/PhysRevB.99.060406

Introduction. Skyrmionics has attracted enormous interest over the recent years, as skyrmions [1–5]—small magnetic quasiparticles that are topologically protected—are aspirants to be "bits" in future data storage devices [6–16]. The integral of the local spin chirality

$$n_{\mathrm{Sk}}(\boldsymbol{r}) = \boldsymbol{s}(\boldsymbol{r}) \cdot \left(\frac{\partial \boldsymbol{s}(\boldsymbol{r})}{\partial x} \times \frac{\partial \boldsymbol{s}(\boldsymbol{r})}{\partial y} \right) \tag{1}$$

of a skyrmion with magnetic texture $\boldsymbol{s}(\boldsymbol{r})$ tells the skyrmion number $N_{\mathrm{Sk}} = \pm 1$ [17,18], that is, the topological invariant which characterizes skyrmions and antiskyrmions [19–22], respectively. On top of this, $n_{\mathrm{Sk}}(\boldsymbol{r})$ induces a topological Hall effect (THE) [23–34], which is an additional contribution to the Hall effect [35] of electrons in skyrmion crystals (SkXs, a periodic array of skyrmions; Fig. 1).

Another quantity related to the magnetic texture is the orbital magnetization, which is explained in a semiclassical picture by the circulation of conduction electrons in the presence of spin-orbit coupling (SOC) [36–41]. Recently, it has been shown that spin chirality, for example, in SkXs, can as well induce an orbital magnetization, even without SOC [42–44].

In this Rapid Communication, we establish a complete scheme (Fig. 1) for identifying the type of SkX in an experiment, without reverting to real-space imaging (e.g., Lorentz microscopy [45]). The TH conductivity and the orbital magnetization describe the THE and are proportional to N_{Sk}; therefore they differentiate skyrmions from antiskyrmions. Furthermore, we predict a magnetoelectric effect in SkXs, which is within experimental reach; the magnetoelectric polarizability [46–48] and the spin toroidization [49,50] allow one to determine the skyrmion helicity, by which Néel skyrmions are differentiated from Bloch skyrmions. While the THE quantities are based on reciprocal space Berry curvature, the magnetoelectric effect is characterized by the mixed Berry curvature analogs (Fig. 1).

Model and methods. We consider a two-dimensional square lattice with a fixed skyrmion texture $\{\boldsymbol{s}_i\}$ (unit length, i lattice site). The resulting skyrmions and antiskyrmions can have various helicities [cf. Figs. 1(c)–1(e)].

The electrons in the SkX are described by a tight-binding Hamiltonian

$$H = \sum_{ij} t\, c_i^\dagger\, c_j + m \sum_i \boldsymbol{s}_i \cdot (c_i^\dagger \boldsymbol{\sigma} c_i) \tag{2}$$

($c_i^\dagger$ and c_j creation and annihilation operators, respectively), with Hund's rule coupling. The electron spins interact with the magnetic texture (m coupling energy; $\boldsymbol{s}_i$ unit vector; $\boldsymbol{\sigma}$ vector of Pauli matrices), which could be created by localized d electrons that are not explicitly featured in this one-orbital Hamiltonian.

From the eigenvalues $E_n(\boldsymbol{k})$ and eigenvectors $|u_n(\boldsymbol{k})\rangle$ of the Hamiltonian (2) we calculate the $\boldsymbol{k}$ space and the mixed Berry curvature for band n,

$$\Omega_n^{(ij)}(\boldsymbol{k}) = -2\,\mathrm{Im}\left\langle \partial_{k_i} u_n(\boldsymbol{k}) \middle| \partial_{k_j} u_n(\boldsymbol{k}) \right\rangle, \tag{3a}$$

$$D_n^{(ij)}(\boldsymbol{k}) = -2\,\mathrm{Im}\left\langle \partial_{k_i} u_n(\boldsymbol{k}) \middle| \frac{1}{m} \partial_{s_j} u_n(\boldsymbol{k}) \right\rangle, \tag{3b}$$

respectively. With

$$v_{nl}^{(j)}(\boldsymbol{k}) \equiv \langle u_n(\boldsymbol{k}) | \partial_{k_j} H(\boldsymbol{k}) | u_l(\boldsymbol{k}) \rangle\,, \tag{4a}$$

$$s_{nl}^{(j)}(\boldsymbol{k}) \equiv \langle u_n(\boldsymbol{k}) | \sigma_j | u_l(\boldsymbol{k}) \rangle \tag{4b}$$

*Corresponding author: bgoebel@mpi-halle.mpg.de

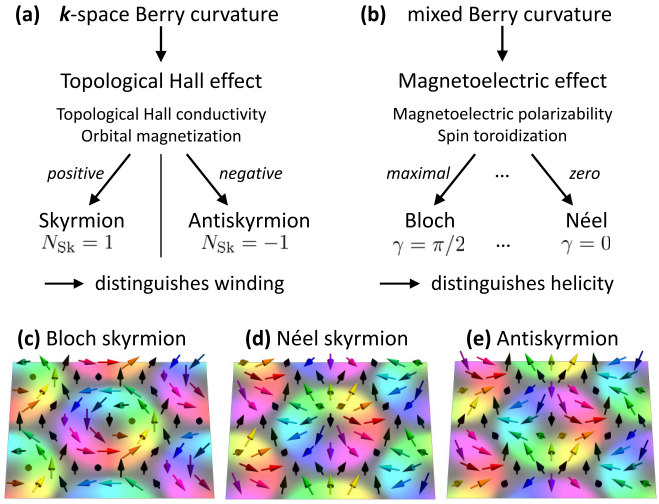

FIG. 1. Core message of this Rapid Communication. (a) Skyrmions and antiskyrmions are distinguished by the topological Hall effect. (b) The helicity of skyrmions (e.g., Bloch and Néel skyrmions) is differentiated by the magnetoelectric effect. With these quantities, (c) Bloch skyrmions, (d) Néel skyrmions, and (e) antiskyrmions can be distinguished. The color scale in (c)–(e) indicates the in-plane orientation of the spins (arrows).

$(j = x, y, z)$, we arrive at

$$\Omega_n^{(ij)}(\boldsymbol{k}) = -2\,\mathrm{Im}\sum_{l\neq n}\frac{v_{nl}^{(i)}(\boldsymbol{k})v_{ln}^{(j)}(\boldsymbol{k})}{[E_n(\boldsymbol{k}) - E_l(\boldsymbol{k})]^2}, \tag{5a}$$

$$D_n^{(ij)}(\boldsymbol{k}) = -2\,\mathrm{Im}\sum_{l\neq n}\frac{v_{nl}^{(i)}(\boldsymbol{k})s_{ln}^{(j)}(\boldsymbol{k})}{[E_n(\boldsymbol{k}) - E_l(\boldsymbol{k})]^2}. \tag{5b}$$

Integration over the occupied states [shorthand notation $\int_{\mathrm{occ}}(\cdot) \equiv \sum_n \int(\cdot)\Theta(E_n(\boldsymbol{k}) - E_\mathrm{F})d^2k$ with E_F Fermi energy and Θ Fermi distribution at zero temperature] yields the conductivity σ_{ij} [51] and the magnetoelectric polarizability α_{ij} [47–49],

$$\sigma_{ij}(E_\mathrm{F}) = -\frac{e^2}{h}\frac{1}{2\pi}\int_{\mathrm{occ}}\Omega_n^{(ij)}(\boldsymbol{k}), \tag{6a}$$

$$\alpha_{ij}(E_\mathrm{F}) = g\mu_\mathrm{B}\frac{e}{(2\pi)^2}\int_{\mathrm{occ}}D_n^{(ij)}(\boldsymbol{k}). \tag{6b}$$

From the orbital magnetic moment [36,37]

$$\boldsymbol{m}_n(\boldsymbol{k}) = -\frac{e}{2\hbar}\,\mathrm{Im}\sum_{l\neq n}\frac{\boldsymbol{v}_{nl}(\boldsymbol{k})\times\boldsymbol{v}_{ln}(\boldsymbol{k})}{E_n(\boldsymbol{k}) - E_l(\boldsymbol{k})}, \tag{7}$$

we calculate the orbital magnetization [39],

$$M_z(E_\mathrm{F}) = \frac{1}{(2\pi)^2}\int_{\mathrm{occ}}m_n^{(z)}(\boldsymbol{k}) + \frac{e}{\hbar}\frac{1}{(2\pi)^2} \times\int_{\mathrm{occ}}\frac{\Omega_n^{(xy)}(\boldsymbol{k}) - \Omega_n^{(yx)}(\boldsymbol{k})}{2}[E_\mathrm{F} - E_n(\boldsymbol{k})]; \tag{8}$$

likewise, from the spin toroidal moment,

$$\boldsymbol{t}_n(\boldsymbol{k}) = \frac{g\mu_\mathrm{B}}{2}\,\mathrm{Im}\sum_{l\neq n}\frac{\boldsymbol{v}_{nl}(\boldsymbol{k})\times\boldsymbol{s}_{ln}}{E_n(\boldsymbol{k}) - E_l(\boldsymbol{k})}, \tag{9}$$

the spin toroidization, as recently shown by Gao *et al.* [49],

$$T_z(E_\mathrm{F}) = \frac{1}{(2\pi)^2}\int_{\mathrm{occ}}t_n^{(z)}(\boldsymbol{k}) - g\mu_\mathrm{B}\frac{1}{(2\pi)^2} \times\int_{\mathrm{occ}}\frac{D_n^{(xy)}(\boldsymbol{k}) - D_n^{(yx)}(\boldsymbol{k})}{2}[E_\mathrm{F} - E_n(\boldsymbol{k})]. \tag{10}$$

The terms with $m_n^{(z)}$ and $t_n^{(z)}$ capture the intrinsic contributions of each Bloch electron, while the other terms account for the Berry curvatures $\Omega_n^{(ij)}$ and $D_n^{(ij)}$, which modify the density of states [39].

Topological Hall effect as a quantum Hall effect. Before discussing the novel results concerning the energy-dependent orbital magnetization, magnetoelectric polarizability, and spin toroidization, a sketch of the band formation and the TH conductivity is adequate; cf. Refs. [30,31].

For $m = 0$ in the Hamiltonian (2), the so-called zero-field band structure is spin degenerate because there is neither spin-orbit coupling nor coupling to the SkX magnetic texture.

If m is turned on, the spin degeneracy is lifted and the electron spins tend to align locally parallel or antiparallel with the magnetic texture. At $m \approx 5t$ the spin alignment is almost complete and two blocks with n_b (number of sites forming a SkX unit cell) bands each are formed: one for parallel (higher energies) and one for antiparallel alignment (lower energies); see Fig. 2(a).

In the limit $m \to \infty$ the alignment is perfect and the electron spins follow the skyrmion texture adiabatically. Both blocks are identical but shifted in energy. Roughly speaking, besides the rigid shift by $\pm m$, the nontrivial Zeeman term leads to a "condensation" of bands [identified as Landau levels (LLs) in what follows].

The perfect alignment for $m \to \infty$ motivates the transformation of the Hamiltonian (2): A local spin rotation diagonalizes the Zeeman term [29–31,52] and alters the hopping term (the hopping strengths t_{ij} become complex 2×2 matrices). Since the system can be viewed as consisting of two (uncoupled) spin species, it is sufficient to consider only one species. The resulting Hamiltonian describes a spin-polarized version of the quantum Hall effect (QHE). Since we discuss charge conductivities, the diagonal Zeeman term is dropped and we arrive at the Hamiltonian

$$H_\parallel = \sum_{ij}t_{ij}^{(\mathrm{eff})}\,\tilde{c}_i^\dagger\,\tilde{c}_j \tag{11}$$

of a quantum Hall (QH) system (spinless electrons on a lattice) [53–59]. The effective hopping strengths $t_{ij}^{(\mathrm{eff})}$ describe the coupling of the electron charges with a collinear inhomogeneous magnetic field,

$$B_\mathrm{em}^{(z)}(\boldsymbol{r}) \propto n_\mathrm{Sk}(\boldsymbol{r}). \tag{12}$$

This emergent field [17,18] is given by the spin chirality (1), that is, the real-space Berry curvature in the continuous limit [17,18]. The parallel (antiparallel) alignment of the electron spins, corresponding to the upper (lower) block in the band structure for $m \to \infty$, manifests itself in the sign of the nonzero average of B_em.

For finite m, the mapping of the THE onto the QHE—and the one-to-one identification of bands and LLs—is reasonable as long as the band blocks are separated, i.e., for $m \geqslant 4t$ [60].

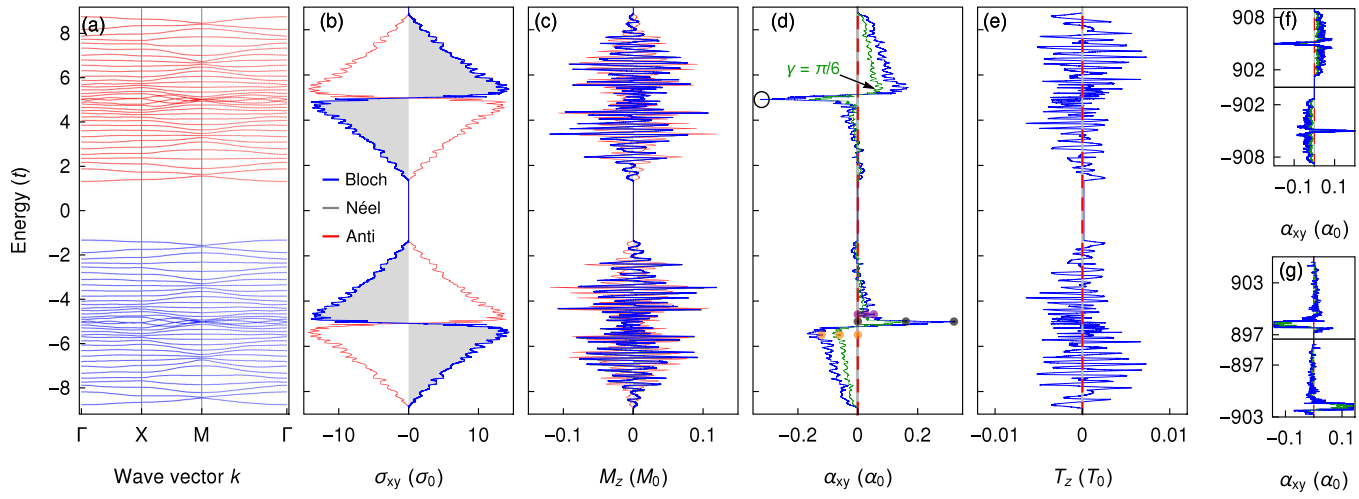

FIG. 2. Properties of a skyrmion crystal. Parameters read $n_b = 36$ (sites in the skyrmion unit cell), coupling $m = 5t$. A Bloch ($N_{Sk} = +1$, $\gamma = \pi/2$; topological charge and helicity), a Néel ($N_{Sk} = +1$, $\gamma = 0$), and an antiskyrmion ($N_{Sk} = -1$, $\gamma = 0$) are compared. (a) Band structure, (b) TH conductivity σ_{xy}, (c) orbital magnetization M_z, (d) magnetoelectric polarizability α_{xy}, and (e) spin toroidization T_z are separated into blocks in which the electron spins are aligned parallel [red in (a)] or antiparallel (blue) with the skyrmion magnetic texture ($\sigma_0 \equiv e^2/h$, $M_0 \equiv te/\hbar$, $\alpha_0 \equiv g\mu_B e/at$, and $T_0 \equiv g\mu_B/a$; a is the lattice constant). The band structure is identical for all skyrmion types. In (d) results for an intermediate skyrmion with $\gamma = \pi/6$ are shown in addition (green). Colored dots refer to Fig. 3. (f) α_{xy} in the strong-coupling limit $m = 900t$ and (g) for larger skyrmions $n_b = 48$ on a different lattice (triangular).

The LL character of the bands arises in Chern numbers and in the TH conductivity [Fig. 2(b)]. Bands of the upper (lower) block carry Chern numbers of $+1$ (-1) due to the positive (negative) average emergent field. As a result, the TH conductivity is quantized in steps of e^2/h. At the shifted van Hove singularity (VHS) $E_{VHS} = \pm m$, the TH conductivity changes sign in a narrow energy window.

The quantization and the sign change are closely related to the zero-field band structure [30,31,61]. At the VHS the character of the Fermi lines changes from electron- to holelike. The bands close to the VHS are simultaneously formed from electron- and holelike states, leading to a large Chern number that causes this jump.

Having sketched the influences of the zero-field band structure on the THE, we derive consequences for the orbital magnetization.

Orbital magnetization. The block separation manifests itself in the orbital magnetization (8) as well. Its energy dependence within the lower block is similar to that in the upper one but with opposite sign [Fig. 2(c)]; the latter is explained by the alignment of the electron spin with the magnetic texture.

$M_z(E_F)$ shows rapid oscillations with zero crossings within the band gaps, which is explicated as follows. The emergent field leads to a rotation of an electron wave packet around its center of mass. The first term in Eq. (8), given by $\boldsymbol{m}_n(\boldsymbol{k})$, changes continuously within the bands but is constant within the band gaps. In contrast, the phase-space correction due to the Berry curvature [39] (second term) varies continuously in energy. Its slope in the band gaps is determined by the TH conductivity,

$$\frac{\partial}{\partial E_F} M_z(E_F) = \frac{1}{2e}[\sigma_{yx}(E_F) - \sigma_{xy}(E_F)]. \tag{13}$$

Both gauge-invariant contributions are similar in absolute value but differ in sign. Consequently, their small difference leads to one oscillation per band.

For a better understanding we relate the orbital magnetization in a SkX to that of the associated QH system with (almost) dispersionless bands [62–64]. Besides the oscillations we identify a continuous envelope function [62] (Fig. S1 in the Supplemental Material [65]). In the SkX this envelope is "deformed" due to the inhomogeneity of the emergent field. Nevertheless, the spectrum of the QH system is quite similar to that of the SkX.

The influences of the two terms in Eq. (8) show up "undistorted" in the QH system. The orbital magnetic moment per band (entering the first term) decreases (increases) stepwise at energies below (above) the shifted zero-field VHSs at $E_{VHS} \equiv \pm m$ [cf. Fig. S1(c)]. There is no sign change at the VHSs, in contrast to the TH conductivity. Still, a zero-field explanation holds as $\boldsymbol{M}$ is also based on the $\boldsymbol{k}$-space Berry curvature. At energies below a VHS, LLs are formed from electronlike orbits with a fixed common circular direction. At energies above a VHS, holelike orbits are formed in addition. Since these exhibit the opposite circular direction, they contribute with opposite sign. Both contributions result in an extremum at the VHS.

The size and shape of the orbits dictate the magnitude of the contributions of each band. Therefore, on one hand, the oscillation amplitudes in Figs. 2(c) and S1(b) [corresponding to the step heights in Fig. S1(c)] increase with increasing energy distance of the Fermi energy and band edges. On the other hand, the oscillation amplitudes vanish at the VHS. Recall that the Fermi lines have zero curvature at this particular energy.

When exchanging skyrmions with antiskyrmions the sign of the emergent field changes and so does the sign of both the TH conductivity and the orbital magnetization in Figs. 2(b) and 2(c), as both characterize the THE. These quantities

distinguish skyrmions from antiskyrmions but cannot distinguish Bloch and Néel skyrmions.

Magnetoelectric polarizability. The independence of all above quantities on the skyrmions' helicity calls for further characterization: This is met by the magnetoelectric effect described by magnetoelectric polarizability and spin toroidization. Both quantities are derived from the mixed Berry curvature $D_n^{(ij)}$. If the Fermi energy lies between two Landau levels, the system is insulating. In this case, the transverse magnetoelectric polarizability

$$\alpha_{xy} = \left.\frac{\partial M_y}{\partial E_x}\right|_{\boldsymbol{B}=0} = \left.\frac{\partial P_x}{\partial B_y}\right|_{\boldsymbol{E}=0} \tag{14}$$

quantifies the magnetoelectric coupling [46] to in-plane fields that are applied to a sample in the SkX phase: An in-plane magnetization $\boldsymbol{M}$ (polarization $\boldsymbol{P}$) can be modified by an orthogonal in-plane electric field $\boldsymbol{E}$ (magnetic field $\boldsymbol{B}$ [66]). If the Fermi energy lies within a Landau level, the system is metallic and cannot exhibit a polarization. Nevertheless, an in-plane magnetization can be produced by perpendicular in-plane currents that are brought about by an applied electric field. This so-called magnetoelectric effect in metals is equivalent to an intrinsic Edelstein effect [67] and was predicted [48] and confirmed experimentally for UNi_4B [68], which shows a coplanar toroidal order. The Onsager reciprocal effect is the inverse Edelstein effect: the generation of a current via the injection of a nonequilibrium spin polarization.

For a Bloch SkX, the spectrum of the magnetoelectric polarizability $\alpha_{xy}(E_\mathrm{F})$, Eq. (6b), shows a sign reversal of the two separated blocks [Fig. 2(d)]. Although α_{xy} exhibits plateaus, it is not quantized. Around the VHS the curve shows a sharp peak (circle).

For $m \gg t$ the spectrum of each block becomes symmetric [Fig. 2(f)]. Within a block the sign of α_{xy} mostly remains, in contrast to σ_{xy}. The monotonicity, however, is reversed above the VHS, the reason being the exchange of v_{ln} and $\boldsymbol{s}_{ln}$ in Eqs. (5a) and (5b). While the sign of the velocity is given by the electron or hole character, the spin is aligned with the magnetic texture, irrespective of the electronic character of band l. The mixing of electron and hole states in a small energy window about E_VHS leads to a collapse of α_{xy} with a reversed sign for this small energy region. This energy window corresponds to the jump in σ_{xy}.

Spin toroidization. As the magnetoelectric polarizability is related to the TH conductivity, the spin toroidization (10) is related to the orbital magnetization. It comprises two terms: one given by the spin toroidal moments $\boldsymbol{t}_n$, and the other by the phase-space correction due to the mixed Berry curvature. In analogy to Eq. (13), its slope

$$\frac{\partial}{\partial E_\mathrm{F}} T_z(E_\mathrm{F}) = \frac{1}{2e}[\alpha_{yx}(E_\mathrm{F}) - \alpha_{xy}(E_\mathrm{F})]$$

is given by the magnetoelectric polarizability in the band gap [49].

$T_z(E_\mathrm{F})$ oscillates rapidly for the Bloch SkX [Fig. 2(e)]. In the strong-coupling limit $m \gg t$ the shape of the oscillations becomes more pronounced.

Relation to skyrmion helicity. Changing continuously the skyrmion helicity, from Bloch to Néel skyrmions, α_{xy} and T_z are reduced by a Fermi-energy-*independent* factor

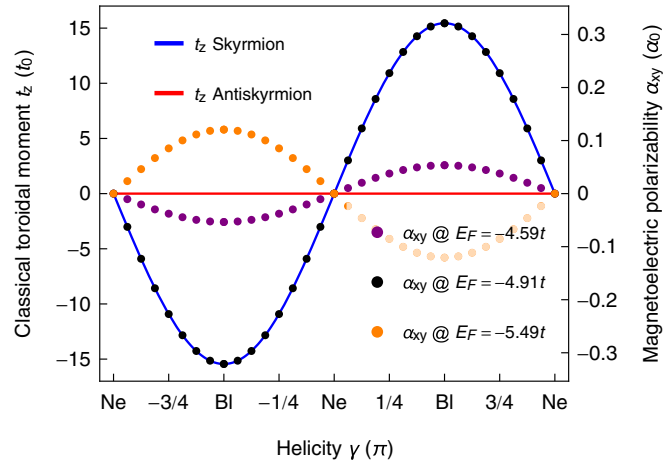

FIG. 3. Dependence of the classical toroidal moment t_z (blue, red) and the magnetoelectric polarizability α_{xy} on the helicity of a skyrmion for selected Fermi energies E_F [distinguished by color, as indicated; also marked in Fig. 2(d)]. t_z is proportional to α_{xy}, with the proportionality factor depending on E_F. $t_0 \equiv g\mu_B a$, $\alpha_0 \equiv g\mu_\mathrm{B} e/at$.

[Fig. 3 and green curve in Fig. 2(d)]; both quantities vanish for Néel SkXs by symmetry. We find that this factor is quantified by the classical toroidal moment [48]

$$\boldsymbol{t} = \frac{g\mu_\mathrm{B}}{2} \sum_i \boldsymbol{r}_i \times \boldsymbol{s}_i \propto \sin(\gamma)\boldsymbol{e}_z \tag{15}$$

($\boldsymbol{r}_i$ position of spin $\boldsymbol{s}_i$ with respect to the skyrmion center). $\boldsymbol{t}$ is a pure real-space quantity given by the skyrmion helicity γ (blue line in Fig. 3). This easily accessible quantity successfully reproduces the functional dependence of α_{xy} (and also of T_z) on the helicity but fails to reproduce the proportionality factor because it does not depend on E_F. Being a classical quantity, $\boldsymbol{t}$ cannot explain the shape of $\alpha_{xy}(E_\mathrm{F})$ and $T_z(E_\mathrm{F})$.

For a Bloch skyrmion ($\gamma = \pi/2$) the full α tensor is antisymmetric ($\alpha_{xy} = -\alpha_{yx}$) and has no longitudinal components. A Néel skyrmion ($\gamma = 0$) exhibits only a longitudinal effect $\alpha_{xx} = \alpha_{yy}$ identical to α_{xy} of the Bloch skyrmion, since all spins are rotated by $\pi/2$ around the z axis [69]. For antiskyrmions Eq. (15) always gives zero. This is why the α tensor is symmetric and T_z is zero in this case. Rotation of the sample always allows one to diagonalize the tensor for antiskyrmion crystals since γ merely orients the two principal axes of an antiskyrmion, for which the texture points into opposite directions giving opposite longitudinal effects $\alpha_{xx} = -\alpha_{yy}$.

The full tensor of the texture-induced magnetoelectric polarizability for a structural square lattice reads

$$\alpha(E_\mathrm{F}) = \alpha_{xy}^{\mathrm{Bloch}}(E_\mathrm{F}) \begin{pmatrix} \cos(\gamma) & \sin(\gamma) \\ -N_\mathrm{Sk}\sin(\gamma) & N_\mathrm{Sk}\cos(\gamma) \end{pmatrix}.$$

The measurement of all tensor elements allows one to determine topological charge N_Sk and helicity γ of an unknown skyrmion.

Conclusion. In this Rapid Communication, we established a complete scheme for the characterization of the skyrmion crystals' topological charge and helicity (Fig. 1). Our findings on the topological Hall effect and the magnetoelectric effect are explained by quite simple pictures: a quantum Hall

system and the classical toroidal moment of a spin texture, respectively.

Our prediction of the helicity-dependent magnetoelectric effect allows one to discriminate Néel and Bloch skyrmions, without reverting to real-space imaging of their magnetic texture (which is in particular difficult for skyrmions arising at interfaces). For an electric field of 10^8 V/m an additional in-plane magnetic moment of one-hundredth of $g\mu_B$ is induced per atom [70]. The collapse of α_{xy} near van Hove singularities is a significant feature and could establish a new hallmark of the SkX phase: It is observable by shifting the Fermi energy (e.g., by a gate voltage or by chemical doping).

As shown in Figs. 2(f) and 2(g) as well as in the Supplemental Material [65], the main claims of this Rapid Communication depend qualitatively neither on skyrmion size, strength of the exchange interaction, nor on the lattice geometry. The established scheme for discrimination (Fig. 1) is a general result, which is not limited to specific materials. All presented quantities arise solely due to coupling of "spinful" electrons with the skyrmion texture and vanish in the absence of skyrmions. The skyrmion-induced contributions are distinguishable from the corresponding nonskyrmionic counterparts, e.g., the anomalous Hall effect in the presence of spin-orbit coupling, the "conventional" magnetization, and the "conventional" magnetoelectric effect in multiferroic materials [14,71–73]).

An experimental proof of the predicted magnetoelectric effect can be done simplest for a nonmultiferroic material with a crystal symmetry that allows only for Bloch skyrmions (e.g., MnSi) [74]. The transverse magnetoelectric effect arises purely due to toroidal order of the SkX and should be measurable in an isolated manner in such a material. The experiment can be conducted in analogy to that of Ref. [68], in which the metallic coplanar toroidal magnet UNi_4B was investigated.

Acknowledgments. We are grateful to Yukitoshi Motome, Gerrit E. W. Bauer, and Annika Johansson for fruitful discussions. This work is supported by Priority Program SPP 1666 and SFB 762 of Deutsche Forschungsgemeinschaft (DFG).

[1] T. H. R. Skyrme, Nucl. Phys. **31**, 556 (1962).
[2] A. N. Bogdanov and D. A. Yablonskii, Zh. Eksp. Teor. Fiz. **95**, 178 (1989) [Sov. Phys. JETP **68**, 101 (1989)].
[3] A. Bogdanov and A. Hubert, J. Magn. Magn. Mater. **138**, 255 (1994).
[4] U. Rößler, A. Bogdanov, and C. Pfleiderer, Nature (London) **442**, 797 (2006).
[5] S. Mühlbauer, B. Binz, F. Jonietz, C. Pfleiderer, A. Rosch, A. Neubauer, R. Georgii, and P. Böni, Science **323**, 915 (2009).
[6] A. Fert, V. Cros, and J. Sampaio, Nat. Nanotechnol. **8**, 152 (2013).
[7] R. Wiesendanger, Nat. Rev. Mater. **1**, 16044 (2016).
[8] N. Romming, C. Hanneken, M. Menzel, J. E. Bickel, B. Wolter, K. von Bergmann, A. Kubetzka, and R. Wiesendanger, Science **341**, 636 (2013).
[9] P.-J. Hsu, A. Kubetzka, A. Finco, N. Romming, K. von Bergmann, and R. Wiesendanger, Nat. Nanotechnol. **12**, 123 (2017).
[10] X. Zhang, M. Ezawa, and Y. Zhou, Sci. Rep. **5**, 9400 (2015).
[11] X. Zhang, Y. Zhou, M. Ezawa, G. Zhao, and W. Zhao, Sci. Rep. **5**, 11369 (2015).
[12] W. Jiang, P. Upadhyaya, W. Zhang, G. Yu, M. B. Jungfleisch, F. Y. Fradin, J. E. Pearson, Y. Tserkovnyak, K. L. Wang, O. Heinonen *et al.*, Science **349**, 283 (2015).
[13] O. Boulle, J. Vogel, H. Yang, S. Pizzini, D. de Souza Chaves, A. Locatelli, T. O. Menteş, A. Sala, L. D. Buda-Prejbeanu, O. Klein *et al.*, Nat. Nanotechnol. **11**, 449 (2016).
[14] S. Seki, X. Yu, S. Ishiwata, and Y. Tokura, Science **336**, 198 (2012).
[15] S. Woo, K. Litzius, B. Krüger, M.-Y. Im, L. Caretta, K. Richter, M. Mann, A. Krone, R. M. Reeve, M. Weigand *et al.*, Nat. Mater. **15**, 501 (2016).
[16] B. Göbel, A. Mook, J. Henk, and I. Mertig, Phys. Rev. B **99**, 020405(R) (2019).
[17] N. Nagaosa and Y. Tokura, Nat. Nanotechnol. **8**, 899 (2013).
[18] K. Everschor-Sitte and M. Sitte, J. Appl. Phys. **115**, 172602 (2014).
[19] A. K. Nayak, V. Kumar, T. Ma, P. Werner, E. Pippel, R. Sahoo, F. Damay, U. K. Rößler, C. Felser, and S. S. Parkin, Nature (London) **548**, 561 (2017).
[20] M. Hoffmann, B. Zimmermann, G. P. Müller, D. Schürhoff, N. S. Kiselev, C. Melcher, and S. Blügel, Nat. Commun. **8**, 308 (2017).
[21] S. Huang, C. Zhou, G. Chen, H. Shen, A. K. Schmid, K. Liu, and Y. Wu, Phys. Rev. B **96**, 144412 (2017).
[22] B. Göbel, A. Mook, J. Henk, I. Mertig, and O. A. Tretiakov, arXiv:1811.07068.
[23] A. Neubauer, C. Pfleiderer, B. Binz, A. Rosch, R. Ritz, P. G. Niklowitz, and P. Böni, Phys. Rev. Lett. **102**, 186602 (2009).
[24] T. Schulz, R. Ritz, A. Bauer, M. Halder, M. Wagner, C. Franz, C. Pfleiderer, K. Everschor, M. Garst, and A. Rosch, Nat. Phys. **8**, 301 (2012).
[25] N. Kanazawa, Y. Onose, T. Arima, D. Okuyama, K. Ohoyama, S. Wakimoto, K. Kakurai, S. Ishiwata, and Y. Tokura, Phys. Rev. Lett. **106**, 156603 (2011).
[26] M. Lee, W. Kang, Y. Onose, Y. Tokura, and N. P. Ong, Phys. Rev. Lett. **102**, 186601 (2009).
[27] Y. Li, N. Kanazawa, X. Z. Yu, A. Tsukazaki, M. Kawasaki, M. Ichikawa, X. F. Jin, F. Kagawa, and Y. Tokura, Phys. Rev. Lett. **110**, 117202 (2013).
[28] P. Bruno, V. K. Dugaev, and M. Taillefumier, Phys. Rev. Lett. **93**, 096806 (2004).
[29] K. Hamamoto, M. Ezawa, and N. Nagaosa, Phys. Rev. B **92**, 115417 (2015).
[30] B. Göbel, A. Mook, J. Henk, and I. Mertig, Phys. Rev. B **95**, 094413 (2017).
[31] B. Göbel, A. Mook, J. Henk, and I. Mertig, New J. Phys. **19**, 063042 (2017).
[32] J. L. Lado and J. Fernández-Rossier, Phys. Rev. B **92**, 115433 (2015).
[33] P. B. Ndiaye, C. A. Akosa, and A. Manchon, Phys. Rev. B **95**, 064426 (2017).
[34] B. Göbel, A. Mook, J. Henk, and I. Mertig, Eur. Phys. J. B **91**, 179 (2018).

[35] E. H. Hall, Am. J. Math. **2**, 287 (1879).
[36] M.-C. Chang and Q. Niu, Phys. Rev. B **53**, 7010 (1996).
[37] A. Raoux, F. Piéchon, J.-N. Fuchs, and G. Montambaux, Phys. Rev. B **91**, 085120 (2015).
[38] J.-P. Hanke, F. Freimuth, A. K. Nandy, H. Zhang, S. Blügel, and Y. Mokrousov, Phys. Rev. B **94**, 121114 (2016).
[39] D. Xiao, J. Shi, and Q. Niu, Phys. Rev. Lett. **95**, 137204 (2005).
[40] T. Thonhauser, D. Ceresoli, D. Vanderbilt, and R. Resta, Phys. Rev. Lett. **95**, 137205 (2005).
[41] D. Ceresoli, T. Thonhauser, D. Vanderbilt, and R. Resta, Phys. Rev. B **74**, 024408 (2006).
[42] M. d. S. Dias, J. Bouaziz, M. Bouhassoune, S. Blügel, and S. Lounis, Nat. Commun. **7**, 13613 (2016).
[43] M. d. S. Dias and S. Lounis, Proc. SPIE **10357**, 103572A (2017).
[44] F. R. Lux, F. Freimuth, S. Blügel, and Y. Mokrousov, Communications Physics **1**, 60 (2018).
[45] X. Yu, Y. Onose, N. Kanazawa, J. Park, J. Han, Y. Matsui, N. Nagaosa, and Y. Tokura, Nature (London) **465**, 901 (2010).
[46] A. M. Essin, J. E. Moore, and D. Vanderbilt, Phys. Rev. Lett. **102**, 146805 (2009).
[47] A. M. Essin, A. M. Turner, J. E. Moore, and D. Vanderbilt, Phys. Rev. B **81**, 205104 (2010).
[48] S. Hayami, H. Kusunose, and Y. Motome, Phys. Rev. B **90**, 024432 (2014).
[49] Y. Gao, D. Vanderbilt, and D. Xiao, Phys. Rev. B **97**, 134423 (2018).
[50] N. A. Spaldin, M. Fiebig, and M. Mostovoy, J. Phys.: Condens. Matter **20**, 434203 (2008).
[51] N. Nagaosa, J. Sinova, S. Onoda, A. MacDonald, and N. Ong, Rev. Mod. Phys. **82**, 1539 (2010).
[52] K. Ohgushi, S. Murakami, and N. Nagaosa, Phys. Rev. B **62**, 6065(R) (2000).
[53] D. R. Hofstadter, Phys. Rev. B **14**, 2239 (1976).
[54] F. H. Claro and G. H. Wannier, Phys. Rev. B **19**, 6068 (1979).
[55] R. Rammal, J. Phys. **46**, 1345 (1985).
[56] F. Claro, Phys. Status Solidi B **104**, K31 (1981).
[57] D. J. Thouless, M. Kohmoto, M. P. Nightingale, and M. den Nijs, Phys. Rev. Lett. **49**, 405 (1982).
[58] Y. Hatsugai, T. Fukui, and H. Aoki, Phys. Rev. B **74**, 205414 (2006).
[59] D. N. Sheng, L. Sheng, and Z. Y. Weng, Phys. Rev. B **73**, 233406 (2006).
[60] Please note that in real materials $m \leqslant 10t$.
[61] B. Göbel, A. Mook, J. Henk, and I. Mertig, Phys. Rev. B **96**, 060406(R) (2017).
[62] O. Gat and J. E. Avron, Phys. Rev. Lett. **91**, 186801 (2003).
[63] Z. Wang and P. Zhang, Phys. Rev. B **76**, 064406 (2007).
[64] Z. Yuan, Z. Wang, Z. Fu, S. Li, and P. Zhang, Sci. China: Phys., Mech. Astron. **55**, 1791 (2012).
[65] See Supplemental Material at http://link.aps.org/supplemental/10.1103/PhysRevB.99.060406 for orbital magnetization of the quantum Hall system and discussion of the four observables for different SkXs.
[66] The magnetic field $\boldsymbol{B}$ is applied in addition to the field that is needed to stabilize the SkX phase.
[67] V. M. Edelstein, Solid State Commun. **73**, 233 (1990).
[68] H. Saito, K. Uenishi, N. Miura, C. Tabata, H. Hidaka, T. Yanagisawa, and H. Amitsuka, J. Phys. Soc. Jpn. **87**, 033702 (2018).
[69] Similar to superexchange-driven magnetoelectricity in magnetic vortices [75].
[70] We used $\alpha_{xy} = 0.1 g \mu_B e/at$ and typical values of $t = 1$ eV and $a = 1$ nm.The electrical field corresponds to the insulating case and has to be replaced by the corresponding electrical currents if the Fermi energy is located within a band.
[71] S. Seki, S. Ishiwata, and Y. Tokura, Phys. Rev. B **86**, 060403 (2012).
[72] I. Kézsmárki, S. Bordács, P. Milde, E. Neuber, L. Eng, J. White, H. M. Rønnow, C. Dewhurst, M. Mochizuki, K. Yanai *et al.*, Nat. Mater. **14**, 1116 (2015).
[73] E. Ruff, S. Widmann, P. Lunkenheimer, V. Tsurkan, S. Bordács, I. Kézsmárki, and A. Loidl, Sci. Adv. **1**, e1500916 (2015).
[74] A. Leonov, T. Monchesky, N. Romming, A. Kubetzka, A. Bogdanov, and R. Wiesendanger, New J. Phys. **18**, 065003 (2016).
[75] K. T. Delaney, M. Mostovoy, and N. A. Spaldin, Phys. Rev. Lett. **102**, 157203 (2009).